Pergamon

Int. J. Solids Structures Vol. 34, No. 2, pp. 177–201, 1997

0020-7683/97 $15.00 + .00

PII: S0020-7683(96)00003-0

ELASTIC MODULI OF BRITTLE MATRIX COMPOSITES WITH INTERFACIAL DEBONDING

F. G. YUAN[1], N. J. PAGANO[2] and X. CAI[1]

[1] Department of Mechanical and Aerospace Engineering, North Carolina State University, Raleigh, NC 27695-7910, U.S.A.

[2] Wright Laboratory, WL/MLBM, Wright-Patterson AFB, OH 45433-7817, U.S.A.

(*Received* 30 *June* 1995; *in revised form* 7 *December* 1995)

Abstract— Elastic moduli of brittle matrix composites with uni-symmetric and doubly-symmetric interfacial debonding are studied.† Traction continuity and displacement continuity conditions are imposed along the boundary of adjacent representative elements. With careful consideration of symmetric and skew-symmetric conditions in the cell, the uni-symmetric and doubly-symmetric debonding cases can be modelled by a half cell or a quarter cell problem, respectively. The RVE boundaries, in general, do not remain straight for the composite under loading. Parametric studies assessing the effect of the debonding angle, the shear moduli ratios in the constituents and the fiber volume fractions on the composite shear moduli are also presented through finite element analyses. Comparison of the shear moduli between the current compatible displacement field and the linear straight boundary displacements of the RVE is addressed. Copyright © 1996 Elsevier Science Ltd.

INTRODUCTION

The mechanical properties of fiber-reinforced composites can be significantly affected by the bond between the fibers and the matrix. In polymer matrix composites, the composite systems consist of brittle fibers such as graphite and boron in relatively soft matrix materials such as epoxy, and a strong fiber/matrix bond is desired. However, in certain brittle matrix composites, the constituents are both brittle in nature, and the fibers are weakly bonded to the matrix. Although this weak bond is detrimental to compressive and transverse strength properties, it is believed to be an important source of enhancing strength and fracture toughness in these composite systems. Recent experimental studies, Prewo *et al.* (1980), Rice (1981), Grande *et al.* (1988), on brittle matrix composites have also shown that the degree of bonding between the fiber and the matrix can dominate their mechanical properties and associated failure modes. In order to achieve optimal performance between strength and stiffness for composite development, the effect of weak bond or debonded interface conditions on the mechanical properties of composite materials needs to be fully understood.

The prediction of the effective mechanical properties of composite materials can be approached in many ways. The viable approach for engineering applications is based on a theory which replaces the actual heterogeneous medium by an equivalent anisotropic homogeneous continuum if the scale of the deformation is sufficiently larger than the characteristic length of the microstructure. By further assuming the periodicity of the microstructure, the effective elastic moduli of the composite are determined by the elastic properties of the constituents and internal geometry of the representative volume element (RVE) or the unit cell. Since the early 1960s many analytical and numerical studies have been carried out on the determination of the elastic properties of composite materials with perfectly bonded interface. Usually, concentric cylinders, square array, hexagonal array are assumed for mathematical models. Hashin and Rosen (1964) provided the lower and upper bounds of elastic moduli based on variational principles. Semi-analytical approaches have

† In the unisymmetric problem considered later, the stresses on the boundary of the RVE lead to resultant forces and moments, as in couple-stress elasticity. The composite stresses here, however, are defined as volume averages over the RVE, so that the couple-stress effects are ignored. The latter will be considered in a subsequent paper.

been treated by Chen and Cheng (1967), Chen (1970, 1971) to evaluate elastic moduli of the composite. A combination of Fourier method and least square method has been employed to match the boundary conditions on the RVE at discrete points. Application of the finite difference and finite element methods to this class of the problem has been made by Adams and Doner (1967a, b) and Foye (1966). Closed form solutions such as the composite cylinder assemblage (CCA) model, self-consistent model or generalized self-consistent scheme (GSCS) have been proposed by Hashin and Rosen (1964), Hill (1965), and Christensen and Lo (1979). However, the solutions may not be valid for high fiber volume fractions or high rigidity of the fibers. Heaton (1968) first proposed the compatible displacement and stress field along the cell boundaries and then used truncated elasticity series Airy stress function solutions to match the continuity conditions at the interface exactly. The composite moduli were evaluated through a point-matching technique along the cell boundary. Recently Sun and Vaidya (1993) predicted elastic moduli of composite by employing periodic displacement conditions along the cell boundaries and using an energy equivalence consideration with a three-dimensional finite element analysis.

The effect of weak bond or debonded interface on the mechanical properties has been recently studied by several investigators. Some simplified models have been proposed to simulate the imperfect interface condition. Pagano and Tandon (1990) developed an approximate model by assuming various interfacial conditions. Several definitions of composite strain were used in the determination of effective moduli. Benveniste (1984, 1985) simulated the interface by imposing the continuity of normal displacements and tractions at the interface while allowing a jump in the tangential displacement and defined composite strain as the so-called "body average" strain, which, as a surface integral, has the same form as the usual definition of composite strain. Takahashi and Chou (1988) used Eshelby's equivalent inclusion method in conjunction with the Mori-Tanaka theorem to predict transverse moduli of the perfect and completely debonded composite. Hashin (1990) simulated the interface condition by linear relations between interface tractions and displacement jumps and used the GSCS model to predict the effective moduli of the composite. Shimansky *et al.* (1989) used a finite element method to predict transverse moduli of the debonded interface in a ceramic matrix composite.

In the following work, an analysis using finite element methods has been applied to fiber reinforced brittle matrix composites in order to predict the influence of the debonded interface on "effective" elastic moduli of the composites. The extent of the debonded interface is simulated by uni-symmetric and doubly-symmetric debonding geometries. The debonded interface is assumed to be completely separated. The shear moduli ratios in the constituents and fiber volume fraction on the composite shear moduli are also studied. The geometrical layout of the composites with periodic rectangular array model is considered in the analysis. The traction continuity and displacement continuity constraint equations are imposed for different deformation modes in order to maintain the geometric compatibility and static equilibrium between neighboring RVE. Finally, the shear moduli predicted from the current compatible displacement field between the edges of the RVE boundary and linear boundary displacements along the RVE are compared.

FORMULATION

A two phase composite with regularly repeating geometry is considered. When the unidirectional reinforced composite is subjected to a uniform macroscopic applied stress, the stress distribution will depend on the properties of the constituents, interfacial conditions and the geometry of representative volume element. A rectangular RVE with dimensions $2a \times 2b$ is shown in Fig. 1. Two different cases of debonding are considered. In the first case, which will be referred to as uni-symmetric debonding, the fiber is perfectly bonded to the matrix except over the interface region $|\theta| \leqslant \alpha$ (Fig. 1a). In the second case, which we will refer to as doubly-symmetric debonding, the fiber is perfectly bonded to the matrix except over the interface region $|\theta| \leqslant \alpha$ and $|\pi - \theta| \leqslant \alpha$ (Fig. 1b). The z-axis coincides with the fiber axis. Under deformation, each RVE in the composite must experience identical

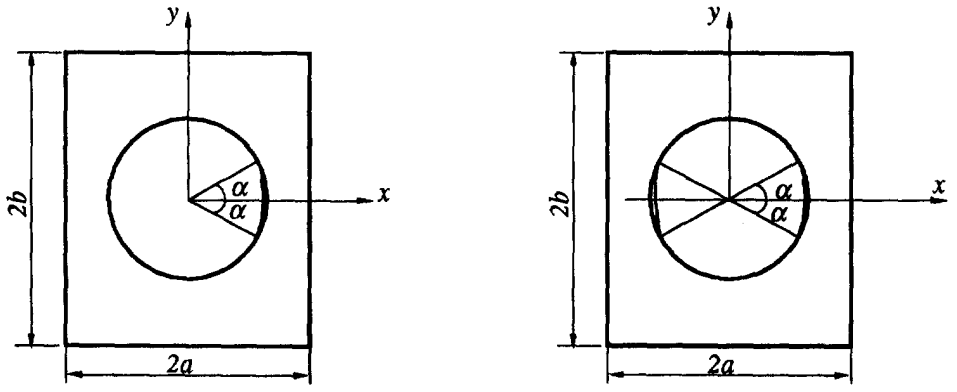

a. Uni-symmetric debonding **b. Doubly-symmetric debonding**

Fig. 1. Interfacial debonding of a representative volume element.

displacement (excluding rigid body displacements) and stress fields. Therefore the constraints must be imposed on the boundary of each cell so that the displacements and stresses are compatible with the displacements and stresses on the neighboring cells.

(*A*) *Young's moduli and Poisson's ratios*

To calculate the Young's moduli and Poisson's ratios of the composite, a periodic rectangular array under generalized plane strain ($\varepsilon_z = \varepsilon_z^0$) but excluding shear loadings is considered. The displacement compatibility conditions on the boundary of the RVE are given as

$$u(a, y) = u(-a, y) + 2a\varepsilon_x^0 \tag{1a}$$

$$v(a, y) = v(-a, y) \tag{1b}$$

$$u(x, b) = u(x, -b) \tag{1c}$$

$$v(x, b) = v(x, -b) + 2b\varepsilon_y^0 \tag{1d}$$

$$w(x, y, z) = \varepsilon_z^0 z \tag{1e}$$

and the traction continuity conditions are given as

$$\sigma_x(a, y) = \sigma_x(-a, y) \tag{2a}$$

$$\tau_{xy}(a, y) = \tau_{xy}(-a, y) \tag{2b}$$

$$\sigma_y(x, b) = \sigma_y(x, -b) \tag{2c}$$

$$\tau_{xy}(x, b) = \tau_{xy}(x, -b). \tag{2d}$$

For uni-symmetric debonding, the problem has symmetric geometry and loading about the x-axis. Hence the deformation field is symmetric about the x-axis. Therefore, we have

$$\varepsilon_x(x, y) = \varepsilon_x(x, -y) \tag{3a}$$

$$\varepsilon_y(x, y) = \varepsilon_y(x, -y) \tag{3b}$$

$$\gamma_{xy}(x, y) = -\gamma_{xy}(x, -y). \tag{3c}$$

Integrating eqns (3a) and (3b) yields

$$u(x, y) = u(x, -y) + f_1(y) \tag{4a}$$

$$v(x, y) = -v(x, -y) + f_2(x). \tag{4b}$$

Substituting eqns (4a) and (4b) into (3c) and imposing the fixed displacements and rotation conditions at the center of the fiber

$$u(0, 0) = v(0, 0) = \omega(0, 0) = 0 \tag{5}$$

where $\omega = \frac{1}{2}[(\partial v/\partial x) - (\partial u/\partial y)]$, we get $f_1(y) = f_2(x) = 0$. That means

$$u(x, y) = u(x, -y) \tag{6a}$$

$$v(x, y) = -v(x, -y). \tag{6b}$$

From eqn (6b), the following condition holds

$$v(x, 0) = 0. \tag{7}$$

Using eqn (6b), eqn (1d) reduces to

$$v(x, b) = b\varepsilon_y^0. \tag{8}$$

Further, from eqn (3c), we have the stress symmetric conditions

$$\tau_{xy}(x, y) = -\tau_{xy}(x, -y). \tag{9}$$

The above equation leads to

$$\tau_{xy}(x, 0) = 0. \tag{10}$$

Combining eqns (2d) and (9) gives

$$\tau_{xy}(x, b) = 0. \tag{11}$$

In summary, the uni-symmetric debonding problem can be solved by half of the RVE cell using the following boundary conditions (eqns (10), (7), (11) and (8))

$$y = 0 \quad \begin{cases} \tau_{xy}(x, 0) = 0 \\ v(x, 0) = 0 \end{cases} \tag{12}$$

$$y = b \quad \begin{cases} \tau_{xy}(x, b) = 0 \\ v(x, b) = b\varepsilon_y^0 \end{cases} \tag{13}$$

together with constraint eqns (1a), (1b), (2a) and (2b).

For the doubly-symmetric debonding, the symmetric characteristics holds about both the x-axis and the y-axis. The overall problem can be modeled by a quarter cell of the RVE using the following boundary conditions together with eqns (12) and (13)

$$x = 0 \quad \begin{cases} u(0, y) = 0 \\ \tau_{xy}(0, y) = 0 \end{cases} \tag{14}$$

$$x = a \quad \begin{cases} u(a, y) = a\varepsilon_x^0 \\ \tau_{xy}(a, y) = 0 \end{cases}. \tag{15}$$

Note that the RVE remains rectangular after deformation for the doubly-symmetric debonding.

For purpose of determination of composite Young's moduli and Poisson's ratios through the composite constitutive relations, $\bar{\sigma}_i = C_{ij}\bar{\varepsilon}_j$ ($i, j = 1, 2, 3$ or x, y, z), three distinct deformation states ($\varepsilon_x^0, \varepsilon_y^0, \varepsilon_z^0$) are considered separately. The first two states are described by plane strain condition ($\varepsilon_z^0 = 0$) with loadings ε_x^0, $\varepsilon_y^0 = 1, 0$ and $0, 1$, respectively; the third state represents the state of $\varepsilon_z^0 = 1$ with the cell boundary constrained. In the case of the cell under plane strain deformation ($w = 0$) with $\varepsilon_x^0 \neq 0$, $\varepsilon_y^0 = 0$, the average stresses with the help of Gauss' theorem and traction continuity conditions in the following eqns (16a, 16b) are obtained as

$$\bar{\sigma}_x = \frac{1}{4ab}\int_S \sigma_x \, dS = \frac{1}{4ab}\oint x T_x \, ds = \begin{cases} \dfrac{1}{2b}\displaystyle\int_{-b}^{b} \sigma_x(a, y)\, dy & \text{uni-symmetric} \\ \dfrac{1}{b}\displaystyle\int_{0}^{b} \sigma_x(a, y)\, dy & \text{doubly-symmetric} \end{cases} \tag{16a}$$

$$\bar{\sigma}_y = \frac{1}{4ab}\int_S \sigma_y \, dS = \frac{1}{4ab}\oint y T_y \, ds = \begin{cases} \dfrac{1}{2a}\displaystyle\int_{a}^{a} \sigma_y(x, b)\, dx & \text{uni-symmetric} \\ \dfrac{1}{a}\displaystyle\int_{0}^{a} \sigma_y(x, b)\, ds & \text{doubly-symmetric} \end{cases} \tag{16b}$$

$$\bar{\sigma}_z = \frac{1}{4ab}\int_S \sigma_z \, dS \tag{16c}$$

where S is the area of the RVE. Due to the debonded interfaces, the line integral $\oint$ should be calculated along the boundary of the RVE as well as the interface between the fiber and matrix. The traction is defined as $T_i = \sigma_{ij} n_j$ ($i, j = x, y$, and z) with n_j being direction cosines of the normal vector on the boundary. Since the tractions are continuous along the bonded interface and are free along the debonded interface, the line integral needs to be evaluated only along outer boundary of the RVE.

The composite strain $\bar{\varepsilon}_x$ is defined as:

$$\bar{\varepsilon}_x = \frac{1}{2a}\int_{-a}^{a} \varepsilon_x(x, b)\, dx = \frac{1}{2a}\int_{-a}^{a} \frac{\partial u}{\partial x}(x, b)\, dx = \frac{1}{2a}[u(a, b) - u(-a, b)] = \varepsilon_x^0. \tag{17}$$

The above derivation is also true for $y = -b$. The definition is appropriate for a strain gage determination. Note that the strain ε_x^0 is not given by the volume average value of ε_x since the displacement u is discontinuous in the RVE [see Pagano and Tandon (1990)]. Alternatively we can define

$$\bar{\varepsilon}_x = \frac{1}{2b}\int_{-b}^{b} \frac{[u(a, y) - u(-a, y)]}{2a}\, dy = \varepsilon_x^0. \tag{18}$$

This definition is based on the averaged displacement gradients on the "ends" of a physical specimen. Both these definitions (which are equivalent) are defined on physical grounds, but they are also identical to Benveniste's "body average" strain definition.

The composite elastic coefficients are then defined as

$$\bar{\sigma}_x \equiv C_{11}\varepsilon_x^0, \quad \bar{\sigma}_y \equiv C_{21}\varepsilon_x^0, \quad \bar{\sigma}_z \equiv C_{31}\varepsilon_x^0. \tag{19}$$

Similarly, $\bar{\varepsilon}_y = \varepsilon_y^0$. Since we are treating generalized plane strain, we have $\bar{\varepsilon}_z = \varepsilon_z^0$. The rest of elastic coefficients can be obtained from the remaining deformation states

$$\bar{\sigma}_x \equiv C_{12}\varepsilon_x^0, \quad \bar{\sigma}_y \equiv C_{22}\varepsilon_y^0, \quad \bar{\sigma}_z \equiv C_{32}\varepsilon_y^0 \tag{20}$$

$$\bar{\sigma}_x \equiv C_{13}\varepsilon_z^0, \quad \bar{\sigma}_y \equiv C_{23}\varepsilon_z^0, \quad \bar{\sigma}_z \equiv C_{33}\varepsilon_z^0. \tag{21}$$

From eqn (9), it is easy to show

$$\bar{\tau}_{xy} = \frac{1}{2b}\int_{b}^{b} \tau_{xy}(a, y)\,\mathrm{d}y = \frac{1}{2b}\left[\int_{0}^{b} \tau_{xy}(a, y)\,\mathrm{d}y + \int_{-b}^{0} \tau_{xy}(a, y)\,\mathrm{d}y\right]$$

$$= \frac{1}{2b}\left[\int_{0}^{b} \tau_{xy}(a, y)\,\mathrm{d}y - \int_{0}^{b} \tau_{xy}(a, y)\,\mathrm{d}y\right] = 0. \tag{22}$$

Notice that for the doubly-symmetric debonding we have $\tau_{xy}(a, y) = 0$ exactly. However, for the uni-symmetric debonding $\tau_{xy}(a, y) \neq 0$, the average shear stress is equal to zero due to the symmetry of τ_{xy} with respect to the x-axis. Therefore we conclude

$$C_{61} = C_{62} = C_{63} = 0. \tag{23}$$

The symmetry of the elastic matrix C_{ij} $(i, j = 1, 2, 3)$ can be easily proved by using the Betti's reciprocal theorem together with traction continuity conditions (Sokolnikoff, 1956). By inverting the elastic matrix, the engineering constants of composite Young's moduli and Poisson's ratios can be attained.

(*B*) *In-plane composite shear modulus*

For the composite under shear, straight cell boundaries may not remain straight after the composite has been deformed. Since the boundary displacements and tractions on any RVE must be compatible with those on the neighboring RVE, for the finite element modeling, constraints are imposed on the displacements at the edges $x =$ constant and $y =$ constant of the cell boundary where the displacements are not necessarily linear. This fact does not seem to have been recognized in the previous literature, even for a perfectly bonded interface. The displacement constraint boundary conditions used in obtaining the in-plane shear moduli for the RVE are given by

$$u(a, y) = u(-a, y) \tag{24a}$$

$$v(a, y) = v(-a, y) + a\gamma_{xy}^0 \tag{24b}$$

$$u(x, b) = u(x, -b) + b\gamma_{xy}^0 \tag{24c}$$

$$v(x, b) = v(x, -b). \tag{24d}$$

Since the in-plane shear is a plane strain problem, we have $w(x, y) = 0$ over the whole RVE. The stress components along the cell boundary are required to satisfy the traction continuity conditions in eqns (2).

For the uni-symmetric debonding, the problem has symmetric geometry and skew-symmetric loadings about the x-axis. Thus the strain components must be skew-symmetric about the x-axis

$$\varepsilon_x(x, y) = -\varepsilon_x(x, -y) \tag{25a}$$

$$\varepsilon_y(x, y) = -\varepsilon_y(x, -y) \tag{25b}$$

$$\gamma_{xy}(x, y) = \gamma_{xy}(x, -y). \tag{25c}$$

Integrating eqns (25a) and (25b) yield

$$u(x, y) = -u(x, -y) + f_3(y) \tag{26a}$$

$$v(x, y) = v(x, -y) + f_4(x). \tag{26b}$$

Substituting eqns (26) into (25c), considering the same condition in eqn (5) as in the previous section, we have $f_3(y) = f_4(x) = 0$. That means

$$u(x, y) = -u(x, -y) \tag{27a}$$

$$v(x, y) = v(x, -y). \tag{27b}$$

Equation (27a) gives

$$u(x, 0) = 0. \tag{28}$$

From eqns (27a) and (24c), we obtain

$$u(x, b) = \tfrac{1}{2} b \gamma_{xy}^0. \tag{29}$$

By applying the isotropic elastic stress–strain relation to eqns (25a) and (25b) for each constituent, we have the skew-symmetric condition for the following stress components

$$\sigma_x(x, y) = -\sigma_x(x, -y) \tag{30a}$$

$$\sigma_y(x, y) = -\sigma_y(x, -y). \tag{30b}$$

The above eqn (30b) gives

$$\sigma_y(x, 0) = 0. \tag{31}$$

Equations (2c) and (30b) yield

$$\sigma_y(x, b) = 0. \tag{32}$$

From eqns (28), (31), (29) and (32), the uni-symmetric debonding case can be analyzed by a half cell using the following conditions

$$y = 0 \quad \begin{cases} u(x, 0) = 0 \\ \sigma_y(x, 0) = 0 \end{cases} \tag{33}$$

$$y = b \quad \begin{cases} u(x, b) = \tfrac{1}{2} b \gamma_{xy}^0 \\ \sigma_y(x, b) = 0 \end{cases} \tag{34}$$

with the eqns (24a), (24b), (2a) and (2b).

For the doubly-symmetric debonding, the problem further exhibits the symmetric geometry and antisymmetric loading about the y-axis. Therefore, the following conditions can be derived in the same manner as eqns (33) and (34)

$$x = 0 \quad \begin{cases} \sigma_x(0, y) = 0 \\ v(0, y) = 0 \end{cases} \tag{35}$$

$$x = a \quad \begin{cases} \sigma_x(a, y) = 0 \\ v(a, y) = \tfrac{1}{2} a \gamma_{xy}^0 \end{cases}. \tag{36}$$

Equations (33–36) give the boundary conditions for the quarter cell calculation under doubly-symmetric debonding conditions.

The deformation due to shear strain at a point under infinitesimal deformation assumes the edges of the element remain straight. This is not the case here. Therefore, we propose the following definition in the spirit of surface averaging:

$$\bar{\gamma}_{xy} = \frac{1}{2a}\int_{a}^{a} \frac{\partial v(x,b)}{\partial x}\,dx + \frac{1}{2b}\int_{-b}^{b} \frac{\partial u(a,y)}{\partial y}\,dy$$

$$= \frac{1}{2a}[v(a,b)-v(-a,b)] + \frac{1}{2b}[u(a,b)-u(a,-b)] = \gamma^0_{xy}. \tag{37}$$

Alternatively we can define

$$\bar{\gamma}_{xy} = \frac{1}{2a}\int_{-a}^{a} \frac{[u(x,b)-u(x,-b)]}{2b}\,dx + \frac{1}{2b}\int_{-b}^{b} \frac{[v(a,y)-v(-a,y)]}{2a}\,dy = \gamma^0_{xy}. \tag{38}$$

It can be seen that the two shear strain definitions of (37) and (38) are identical and equivalent to Benveniste's "body average" shear strain.

Similar to eqn (16), according to Gauss' theorem the average of the in-plane shear stress in the RVE is

$$\bar{\tau}_{xy} = \frac{1}{4ab}\int_S \tau_{xy}\,dS = \frac{1}{4ab}\oint x T_y\,ds = \frac{1}{b}\int_0^b \tau_{xy}(a,y)\,dy \tag{39}$$

where S denotes the area of the unit cell. Note that the eqns (2) and traction continuity have been used to obtain the final form of eqn (39).

The composite in-plane shear modulus is defined as

$$\bar{\tau}_{xy} = G_{12}\bar{\gamma}_{xy} = G_{12}\gamma^0_{xy} = C_{66}\gamma^0_{xy}. \tag{40}$$

From eqns (30a) and (32), it can be shown that

$$\bar{\sigma}_x = \frac{1}{2b}\int_{-b}^{b} \sigma_x(a,y)\,dy = 0$$

$$\bar{\sigma}_y = \frac{1}{2a}\int_{-a}^{a} \sigma_y(x,b)\,dx = 0. \tag{41}$$

Note that for the uni-symmetric debonding case, $\sigma_x(a,y) \neq 0$.† The average stress, however, is equal to zero. For average stress along the z direction, it can be easily shown that

$$\bar{\sigma}_z = \frac{1}{4ab}\int_S \sigma_z\,dS = \frac{1}{4ab}\int_S v(\sigma_x+\sigma_y)\,dS = \frac{1}{4ab}\oint v(xT_x+yT_y)\,ds = 0 \tag{42}$$

due to the antisymmetric nature of the stress distributions. v is either v_m or v_f depending on the region where the integrals are covered. The above relations (41) and (42) indicate

$$C_{16} = C_{26} = C_{36} = 0. \tag{43}$$

It is noticeable that in our model the RVE does not have linear deformation along its

† The moment effect of $\sigma_x(a,y)$, however, is not zero. See first footnote.

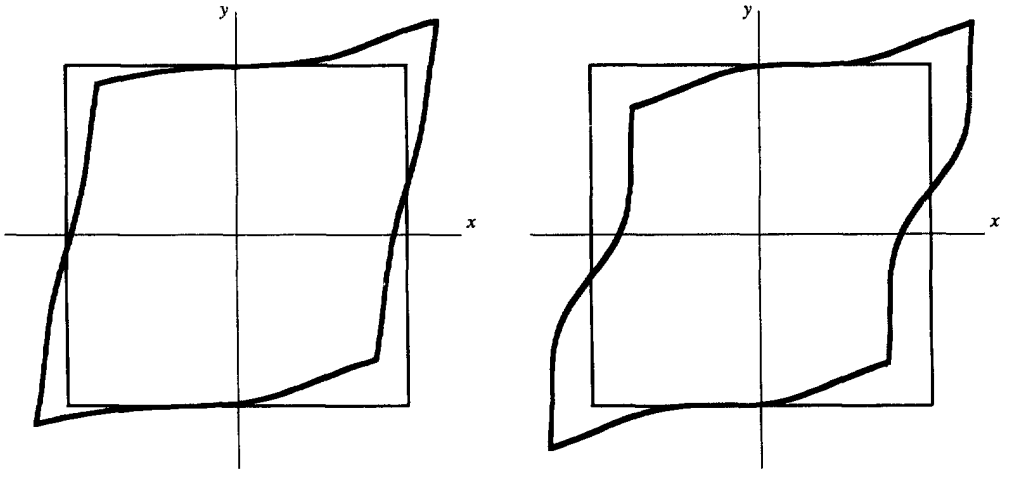

(a) Uni-symmetric (b) Doubly-symmetric

Fig. 2. The in-plane shear deformation profile of RVE.

edge. The typical deformation shape of RVE is sketched in Fig. 2. Figures 2a and b are the deformation of the RVE under in-plane shear for uni-symmetric and doubly-symmetric debonding, respectively (the shear forces of identical magnitude are applied to both cases, the deformed shapes have been magnified with the same factors). Previous studies such as Hashin and Rosen (1964) utilizing straight line displacement fields ($u_i|_{\text{on the boundary}} = \varepsilon^0_{ij}x_j$, where ε^0_{12} is the only nonzero component for in-plane shear) along the cell boundaries lead to the coupling of the moduli in composites, i.e., quantities in eqn (43) are not equal to zero.

(*C*) *Longitudinal composite shear moduli*

For the longitudinal shear problem, the only nonvanishing displacement component is w. The equations of elasticity for the fiber and the matrix both reduce to the Laplace equation, $\nabla^2 w = 0$.

(1) In determining longitudinal shear modulus G_{13} the following constraint boundary conditions for the RVE are imposed

$$w(a, y) = w(-a, y) + 2a\gamma^0_{xz} \tag{44a}$$

$$w(x, b) = w(x, -b) \tag{44b}$$

and the following conditions of shear stresses on the cell boundary need to be satisfied

$$\tau_{xz}(a, y) = \tau_{xz}(-a, y) \tag{45a}$$

$$\tau_{yz}(x, b) = \tau_{yz}(x, -b). \tag{45b}$$

For uni-symmetric debonding, the problem is symmetric about the x-axis. The strain symmetric conditions give

$$\gamma_{xz}(x, y) = \gamma_{xz}(x, -y) \tag{46a}$$

$$\gamma_{yz}(x, y) = -\gamma_{yz}(x, -y). \tag{46b}$$

Hence the stress component should satisfy the following symmetric condition

$$\tau_{yz}(x, y) = -\tau_{yz}(x, -y). \tag{47}$$

The eqn (47) yields

$$\tau_{yz}(x,0) = 0. \tag{48}$$

Combining eqns (45b) and (47), we have

$$\tau_{yz}(x,b) = 0. \tag{49}$$

Therefore, for the uni-symmetric debonding case, the problem can be solved by half of the cell using (48), (49) with (44a) and (45a) as boundary conditions.

For doubly-symmetric debonding, the problem has additional symmetric geometry and antisymmetric loadings about the y-axis. The problem thus has skew-symmetric stress and strain components about the y-axis

$$\gamma_{xz}(x,y) = \gamma_{xz}(-x,y) \tag{50a}$$

$$\gamma_{yz}(x,y) = -\gamma_{yz}(-x,y). \tag{50b}$$

Integrating eqns (50) yields

$$w(x,y) = -w(-x,y)+f_5(y) \tag{51a}$$

$$w(x,y) = -w(-x,y)+f_6(x). \tag{51b}$$

Combining eqns (51a) and (51b), with the consideration of the constraint at the center of the fiber, $w(0,0) = 0$, we have $f_5(y) = f_6(x) = 0$. That means

$$w(x,y) = -w(-x,y). \tag{52}$$

Equation (53) gives

$$w(0,y) = 0. \tag{53}$$

Combining with eqns (44a) and (52) leads to

$$w(a,y) = a\gamma_{xz}^0. \tag{54}$$

Therefore, for doubly-symmetric debonding case, the problem can be solved by a quarter cell RVE with (53), (54), (48) and (49) as the boundary conditions.

The composite longitudinal shear strain can be defined in the following two ways

$$\bar{\gamma}_{xz} = \frac{1}{2a}\int_{-a}^{a}\gamma_{xz}(x,b)\,\mathrm{d}x = \frac{1}{2a}\int_{-a}^{a}\frac{\partial w}{\partial x}(x,b)\,\mathrm{d}x = \frac{1}{2a}[w(a,b)-w(-a,b)] = \gamma_{xz}^0 \tag{55}$$

or

$$\bar{\gamma}_{xz} = \frac{1}{2b}\int_{-b}^{b}\frac{[w(a,y)-w(-a,y)]}{2a}\,\mathrm{d}y = \gamma_{xz}^0. \tag{56}$$

Again, the two definitions of composite shear strains are identical. The average shear stress in the RVE with the help of Gauss theorem is

$$\bar{\tau}_{xz} = \frac{1}{4ab}\int_S \tau_{xz}\,\mathrm{d}S = \frac{1}{4ab}\oint xT_z\,\mathrm{d}s$$

$$= \frac{1}{2b}\int_{-b}^{b}\tau_{xz}(a,y)\,\mathrm{d}y = \frac{1}{b}\int_0^b \tau_{xz}(a,y)\,\mathrm{d}y. \tag{57}$$

The derivation of above equation is similar to that of eqn (16). Equations (45) and the completely separated interface condition have been employed to obtain the final form of eqn (57). Then the composite shear modulus G_{13} is defined as

$$\bar{\tau}_{xz} = G_{13}\bar{\gamma}_{xz} = G_{13}\gamma^0_{xz} = C_{55}\gamma^0_{xz}. \tag{58}$$

From eqn (49) we obtain

$$\bar{\tau}_{yz} = \frac{1}{4ab}\int_S \tau_{yz}\,\mathrm{d}S = \frac{1}{4ab}\oint yT_z\,\mathrm{d}s = \frac{1}{2a}\int_{-a}^{a} \tau_{yz}(x,b)\,\mathrm{d}x = 0. \tag{59}$$

Actually, the shear stress τ_{yz} equals zero exactly along the $y = b$ edge for both the uni-symmetric and doubly-symmetric debonding cases. Hence, the coupling constant is

$$C_{45} = \frac{\bar{\tau}_{yz}}{\gamma^0_{xz}} = 0. \tag{60}$$

(2) The determination of G_{23} is similar to that of G_{13}. The following displacement constraints are imposed

$$w(x,b) = w(x,-b) + 2b\gamma^0_{yz} \tag{61a}$$

$$w(a,y) = w(-a,y) \tag{61b}$$

as well as the stress continuity conditions in eqns (45).

For the uni-symmetric debonding, the deformation field is skew-symmetric about the x-axis.

$$\gamma_{xz}(x,y) = -\gamma_{xz}(x,-y) \tag{62a}$$

$$\gamma_{yz}(x,y) = \gamma_{yz}(x,-y). \tag{62b}$$

From eqn (62a)

$$\gamma_{xz}(x,0) = 0. \tag{63}$$

Integrating eqn (64) and considering the condition $w(0,0) = 0$ lead to

$$w(x,0) = 0. \tag{64}$$

Further integrating eqn (62b) with eqn (64)

$$w(x,y) = -w(x,-y). \tag{65}$$

Combining eqns (61a) and (65)

$$w(x,b) = b\gamma^0_{yz}. \tag{66}$$

Equation (66) clearly shows that the upper and lower edges of the RVE remain straight after deformation. Furthermore, the problem can be analyzed by half of the RVE using

$$\begin{aligned} &y = 0 \quad w(x,0) = 0 \\ &y = b \quad w(x,b) = b\gamma^0_{yz} \end{aligned} \tag{67}$$

and eqns (61b) and (45a) as boundary conditions.

For the doubly-symmetric debonding, the deformation is symmetric about the y-axis.

$$\gamma_{xz}(x, y) = -\gamma_{xz}(-x, y) \tag{68a}$$

$$\gamma_{yz}(x, y) = \gamma_{yz}(-x, y). \tag{68b}$$

Integrating the eqns (68a) and (68b)

$$w(x, y) = w(-x, y). \tag{69}$$

It is obvious that (60b) is automatically satisfied. On the other hand, from (68a)

$$\tau_{xz}(x, y) = -\tau_{xz}(-x, y). \tag{70}$$

Equations (45a) and (70) give

$$\tau_{xz}(a, y) = 0. \tag{71}$$

Considering eqn (70) for $x = 0$

$$\tau_{xz}(0, y) = 0. \tag{72}$$

Therefore the doubly-symmetric debonding case can be analyzed using a quarter of RVE with eqns (67), (71) and (72) being the boundary conditions.

The average shear stress in the RVE is defined as

$$\bar{\tau}_{yz} = \frac{1}{4ab}\int_S \tau_{yz}\,\mathrm{d}S = \frac{1}{4ab}\oint yT_z\,\mathrm{d}s = \begin{cases} \dfrac{1}{2a}\displaystyle\int_{-a}^{a} \tau_{yz}(x, b)\,\mathrm{d}x & \text{uni-symmetric} \\ \dfrac{1}{a}\displaystyle\int_{0}^{a} \tau_{yz}(x, b)\,\mathrm{d}x & \text{doubly-symmetric.} \end{cases} \tag{73}$$

The derivation of the above equation is the same as that of eqn (57). The composite shear modulus can be determined as

$$\bar{\tau}_{yz} = G_{23}\gamma^0_{yz} = C_{44}\gamma^0_{yz}. \tag{74}$$

From eqn (62a), we have

$$\tau_{xz}(x, y) = -\tau_{xz}(x, -y). \tag{75}$$

Therefore

$$\bar{\tau}_{xz} = \frac{1}{2b}\int_{-b}^{b} \tau_{xz}(a, y)\,\mathrm{d}y = \frac{1}{2b}\left[\int_{0}^{b} \tau_{xz}(a, y)\,\mathrm{d}y + \int_{-b}^{0} \tau_{xz}(a, y)\,\mathrm{d}y\right]$$

$$= \frac{1}{2b}\left[\int_{0}^{b} \tau_{xz}(a, y)\,\mathrm{d}y - \int_{0}^{b} \tau_{xz}(a, y)\,\mathrm{d}y\right] = 0. \tag{76}$$

Again, for the doubly-symmetric debonding, the stress equals zero exactly. Note that for uni-symmetric debonding case, $\tau_{xz}(a, y) \neq 0$.† In both cases, eqn (74) indicates that the coupling constant is equal to zero

† The moment effect of $\tau_{xz}(a, y)$, however, is not zero. See first footnote.

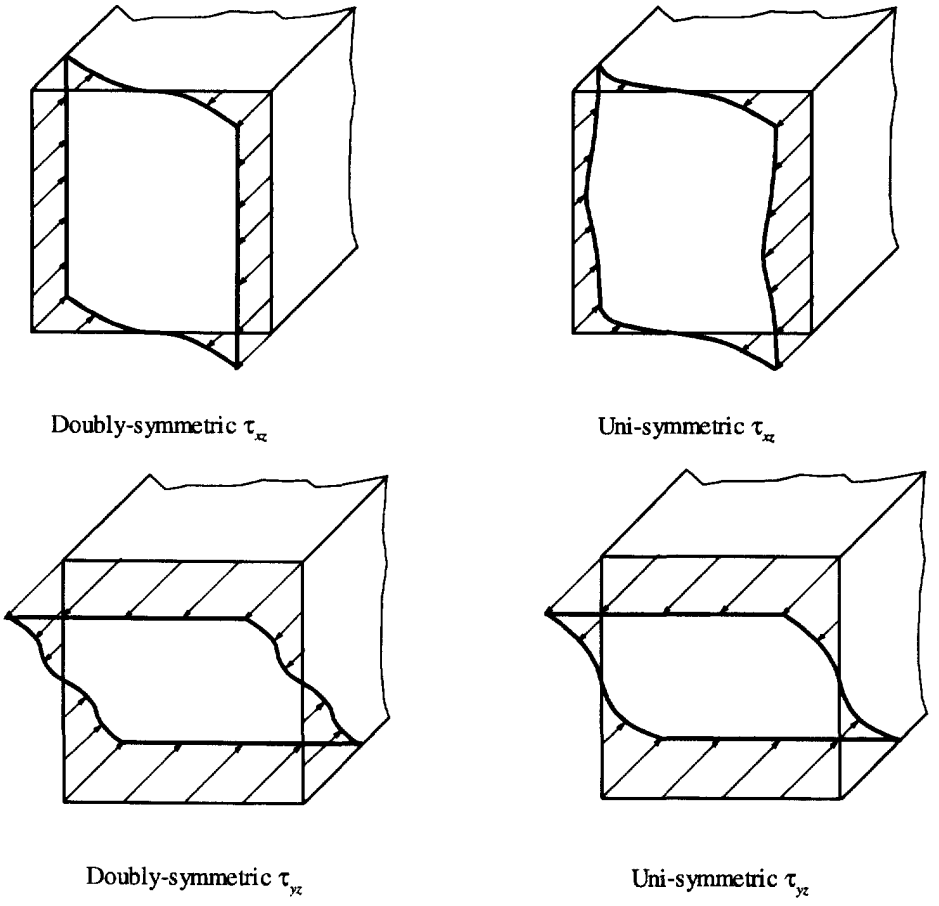

Fig. 3. The longitudinal shear deformation profile of RVE.

$$C_{54} = 0. \tag{77}$$

The problem of calculating the longitudinal shear moduli is mathematically equivalent to that of calculating the effective thermal conductivities of a composite. With displacement w corresponding to temperature, strains γ_{xz}, γ_{yz} corresponding to components of temperature gradient, and stresses τ_{xz}, τ_{yz} corresponding to components of thermal flux q_x and q_y, the composite longitudinal shear moduli are obtained from the analogous heat conduction analysis.

The traction continuity and displacement continuity conditions between the neighboring RVE lead to the nonlinear variation of displacement along the RVE edges. The representative shapes of the deformed RVE under antiplane shear are sketched in Fig. 3.

From eqns (23), (43), (60) and (77), the composite exhibits material characteristics for both uni-symmetric and doubly-symmetric debonding. Furthermore, for the case of debonding without any symmetry, the composite moduli can be determined from the moduli in the uni-symmetric debonding with proper transformation between the global and local axes.

RESULTS AND DISCUSSION

The ANSYS finite element package is selected to analyze the RVE of the periodic rectangular model. For the case of axial extension ε_z^0, the deformation of eqn (1e) is simulated as a thermoelastic problem with thermal expansion coefficients, $\alpha_1 = \alpha_2 = 0$ and $\alpha_3 = \varepsilon_z^0$, for each constituent under unit temperature rise. The problems are modeled as a half cell or quarter cell for the uni-symmetric and doubly-symmetric debonding cases

respectively. Four-node plane element is used in the modeling. Appropriate boundary conditions, as are given in the previous section, are imposed accordingly. The boundary conditions imposed on the surface of a debonded crack are $\sigma_r = \tau_{r\theta} = \tau_{rz} = 0$. These boundary conditions lead to a crack-tip singularity in the exact solution of linear elasticity. They also lead to predicted local overlapping, suggesting closure of the surfaces in the vicinity of the crack tip. Although a correction is possible using contact analysis, the present results are based upon the linear analysis and do not consider such correction. Chao and Laws (1992) have recently shown that under uniaxial loading conditions considering the interface contact results in little difference for the transverse Young's moduli of the composite. Different element sizes with very dense elements around the crack tip are tested during the calculation. Numerical results show that the resolution of mesh around the crack tip has very little influence on the overall moduli.

In the following numerical results, a square periodic array is assumed. In order to illustrate the effect of interfacial debonding on the composite moduli, a brittle Nicalon/1723 Glass ceramic matrix composite with fiber volume fraction 40% is studied unless otherwise mentioned. The fiber and matrix material properties, both assumed to be isotropic, are listed as follows:

Material	E(GPa)	G(GPa)
Nicalon Fiber	200	77
1723 Glass Matrix	88	36

Figures 4–6 depict the effect of debonding angle on the nine composite moduli constants for uni-symmetric debonding case with the x, y and z structural axes shown in Fig. 1 coinciding with the material principal axes 1, 2 and 3. The moduli of composite are presented in terms of engineering constants E_1, E_2, ..., etc. In the extreme cases of perfect bonding, the composite with a square periodic array has only six independent elastic constants; in which $E_1 = E_2$, $G_{13} = G_{23}$, $\nu_{13} = \nu_{23}$. In the notation for Poisson's ratios, ν_{ij} signifies the negative of the ratio of ε_j to ε_i under uniaxial stress σ_i. The numerical results for these constants agree well with the concentric cylinder model solution obtained by Hashin and

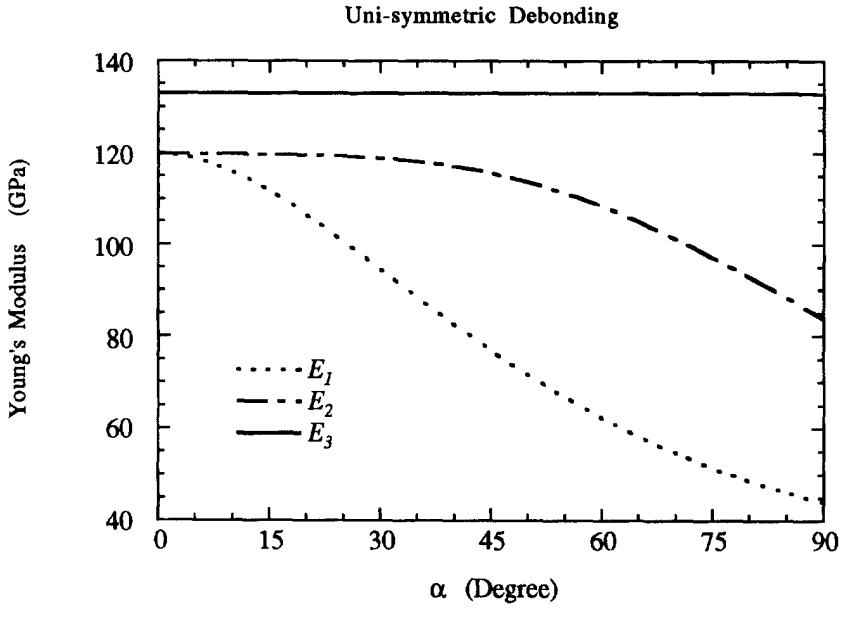

Fig. 4. The effect of debonding angle on the composite Young's moduli for uni-symmetric debonding case.

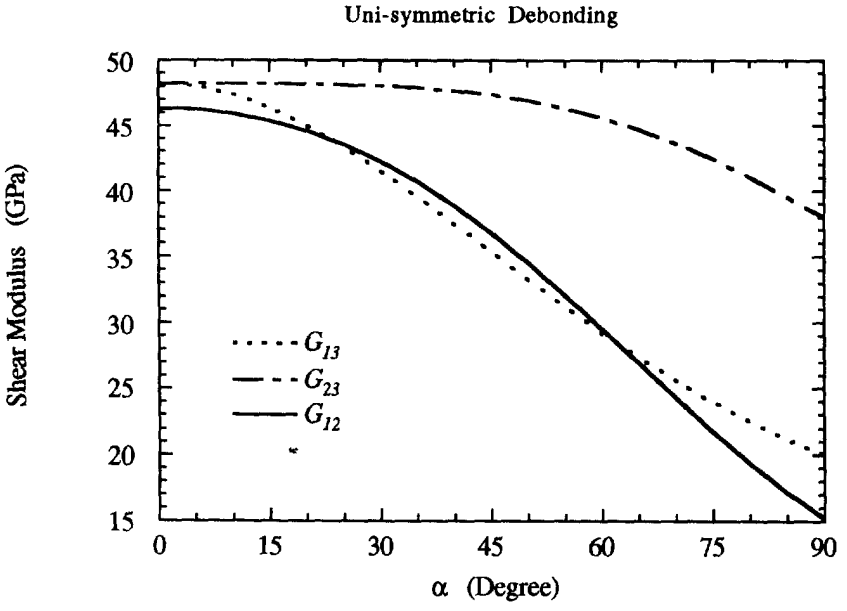

Fig. 5. The effect of debonding angle on the composite shear moduli for uni-symmetric debonding case.

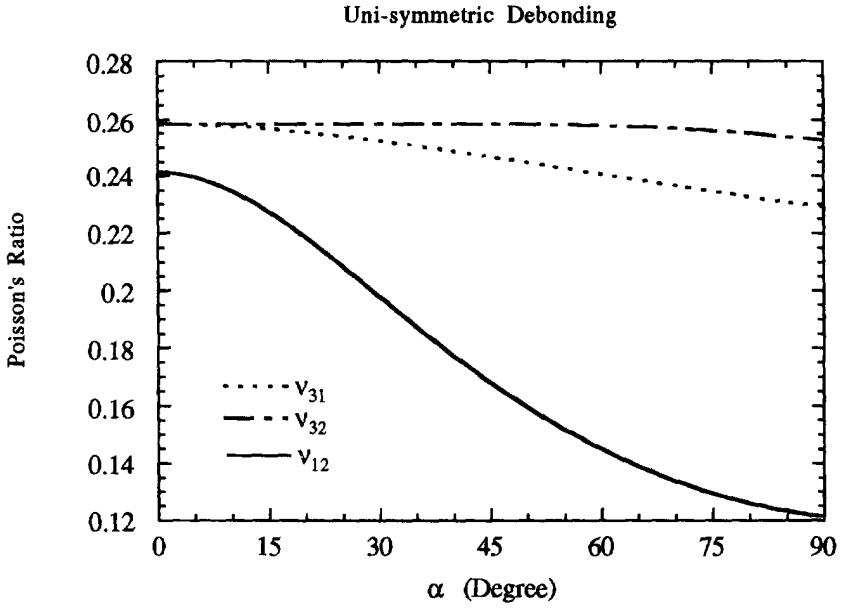

Fig. 6. The effect of debonding angle on the composite Poisson's ratio for uni-symmetric debonding case.

Rosen (1964). As expected, the axial modulus E_3 is insensitive to the debonded interface conditions. The numerical values of E_3 decrease from 133.02 GPa for perfect bonding case to 132.95 GPa for 90° debonding. For engineering applications, the axial modulus can be accurately predicted from the rule of mixtures which gives 132.80 GPa regardless of the bonding between the fiber and the matrix.

The next set of Figs 7–9 illustrates the effect of debonding angle on the composite moduli for doubly-symmetric debonding. There are two extreme cases for the debonding angles. When $\alpha = 0°$ which is the perfectly bonded case, the problem is identical to the case

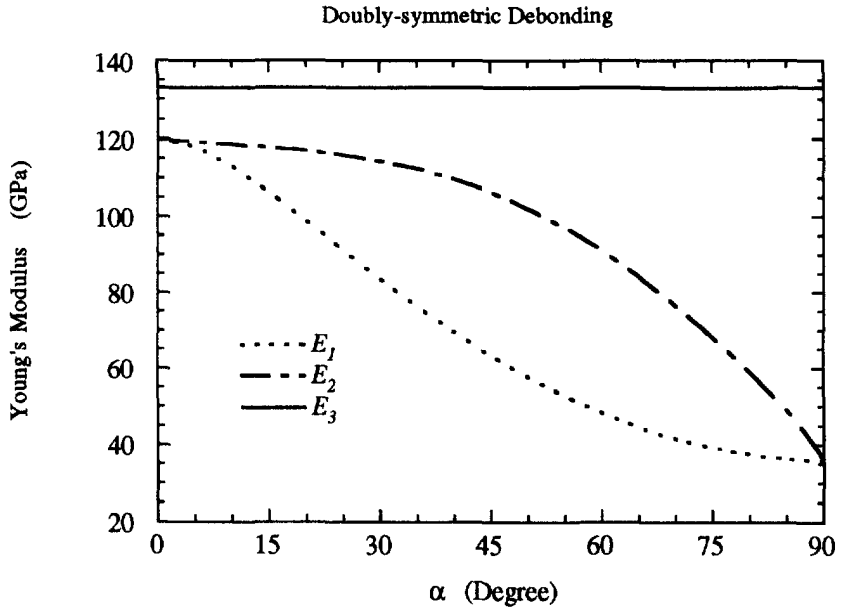

Fig. 7. The effect of debonding angle on the composite Young's moduli for doubly-symmetric debonding case.

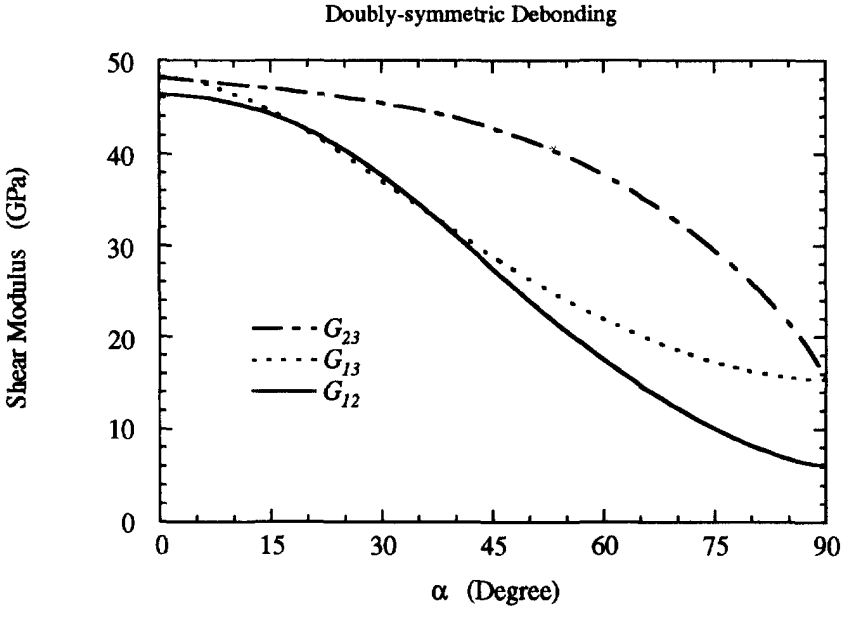

Fig. 8. The effect of debonding angle on the composite shear moduli for doubly-symmetric debonding case.

of uni-symmetric debonding with $\alpha = 0^\circ$. The $\alpha = 90^\circ$ case also presents identical properties along the x and y axis, hence it has only six independent constants. From Fig. 7, it is also clearly shown that the debonding angle has negligible effect on the axial modulus E_3 for doubly-symmetric debonding. Also from Figs 4–9, E_2, G_{23}, ν_{32} and ν_{31} are affected insignificantly by the debonding; Conversely, E_1, G_{13}, G_{12} and ν_{12} are influenced strongly by the debonding at the fiber-matrix boundary.

Parametric studies are conducted for shear moduli of the composite shown in Figs 10–17. In these studies the values of the ratios G_f/G_m varying from 1 to 1000 and five fiber

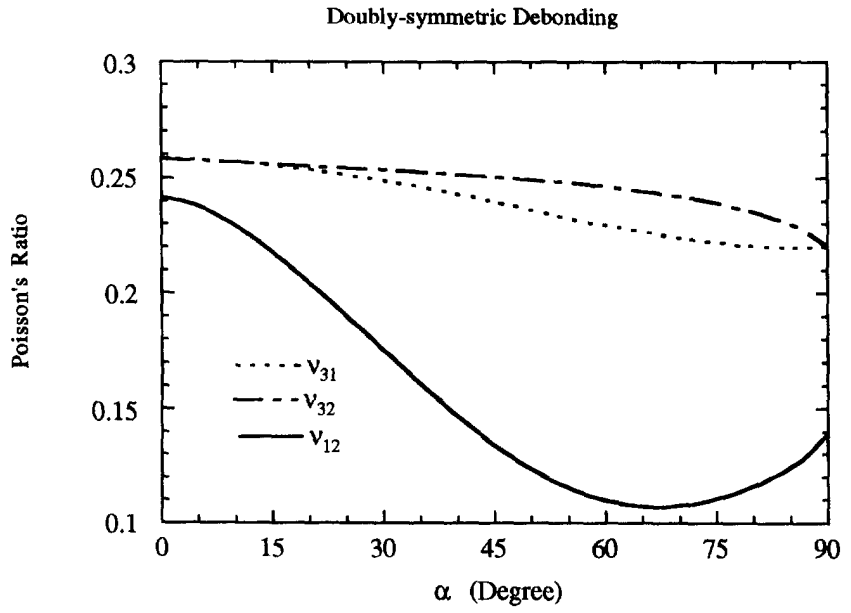

Fig. 9. The effect of debonding angle on the composite Poisson's ratio for doubly-symmetric debonding case.

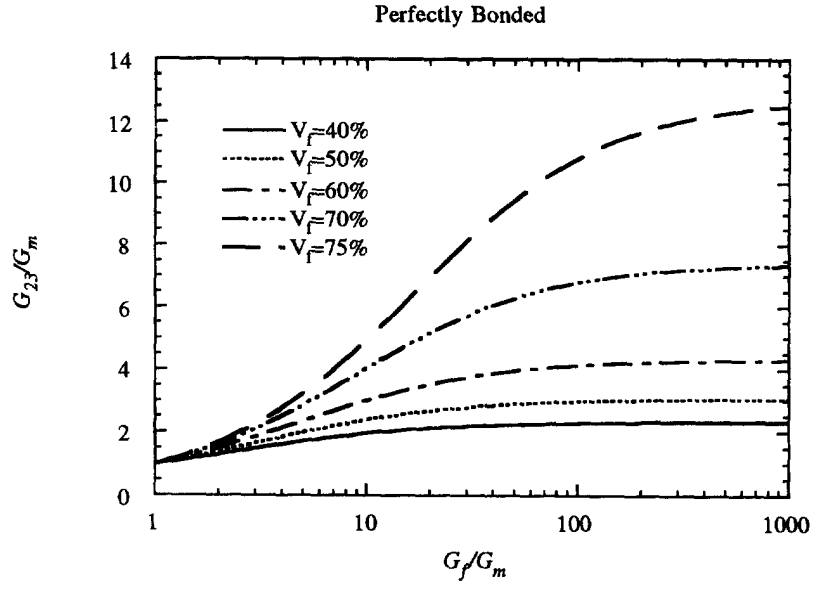

Fig. 10. Effect of fiber volume fraction on the composite shear moduli G_{23} for perfectly bonded interface.

volume fractions covering from 40% to 75% are considered. In calculating G_{12}, the Poisson's ratios of the fiber and the matrix are assumed to be 0.3 and 0.222 respectively. Figures 10–11 illustrate the effect of the ratios G_f/G_m on longitudinal shear modulus G_{23} and in-plane shear moduli G_{12} for a perfectly bonded composite. Notice for perfect bonding, G_{13} is the same as G_{23}. These figures show that the composite moduli approach asymptotic values as the values of G_f/G_m increase.

Figures 12–14 depict the variations of composite shear moduli vs G_f/G_m for 45° uni-symmetrically debonded composite. It can be seen that for this case the degree of debonding causes little change in G_{23}, but it does reduce the other two moduli, G_{13} and G_{12} significantly.

Figures 15–17 illustrate the variation of shear moduli vs G_f/G_m for doubly-symmetric debonding ($\alpha = 45°$). The trend is somewhat reversed for G_{12}. The in-plane composite shear

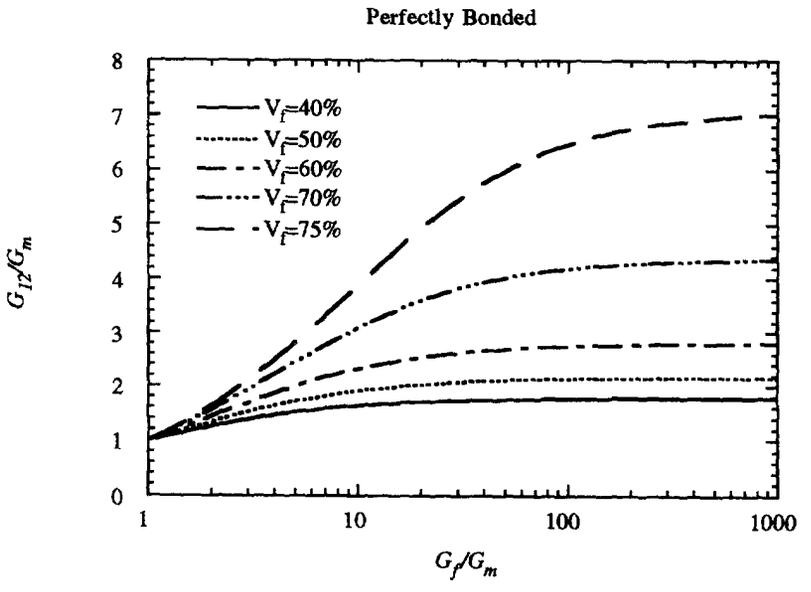

Fig. 11. Effect of fiber volume fraction on the composite shear moduli G_{12} for perfectly bonded interface.

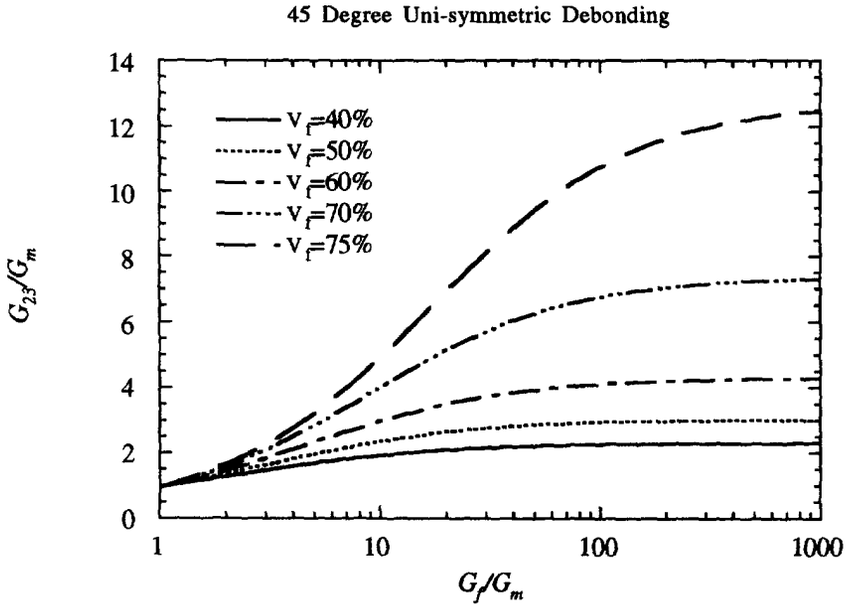

Fig. 12. Effect of fiber volume fraction on the composite shear moduli G_{23} for uni-symmetrically 45° debonded interface.

moduli are lower than the shear modulus of the matrix in the range of the fiber volume fractions studied. The increase of shear modulus of the fiber still causes the increase in the composite modulus; while the increase in the volume fraction of the fiber will decrease the overall modulus of the composite. This phenomena can be interpreted by the fact that the in-plane shear loading is carried primarily by the matrix rather than the fiber for doubly-symmetric debonding composite.

To illustrate the disparity of the composite moduli prediction between our current model with nonlinear compatible deformation among the RVE edges and the model with straight deformation along the RVE edges, numerical results of shear moduli with a 45°

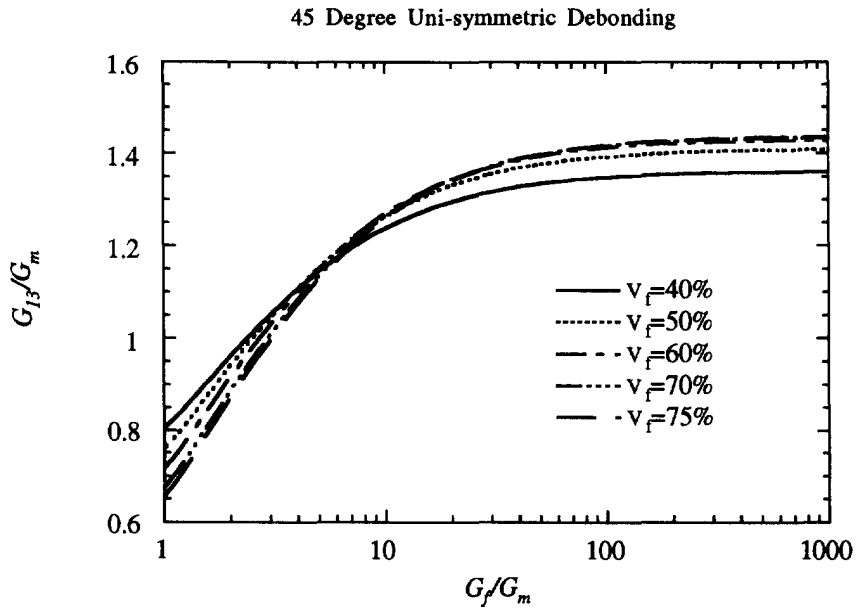

Fig. 13. Effect of fiber volume fraction on the composite shear moduli G_{13} for uni-symmetrically 45° debonded interface.

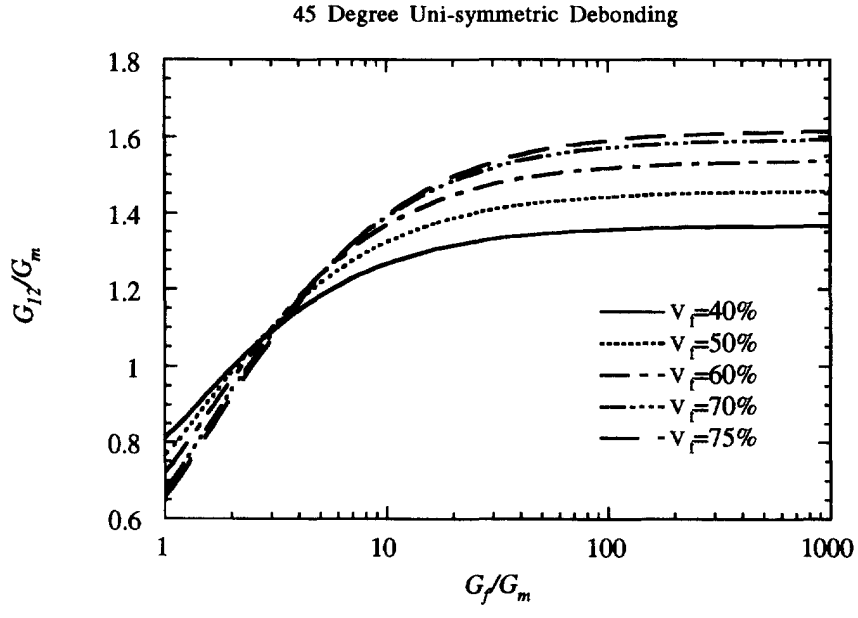

Fig. 14. Effect of fiber volume fraction on the composite shear moduli G_{12} for uni-symmetrically 45° debonded interface.

debonding angle are compared for the two models. In calculating the average shear stresses, definitions similar to eqns (39), (57) and (73) are used for the straight boundaries

$$\bar{\tau}_{xy} = \frac{1}{4ab}\oint xT_y \,\mathrm{d}s = \frac{1}{4ab}\oint yT_x \,\mathrm{d}s$$

$$\bar{\tau}_{yz} = \frac{1}{4ab}\oint yT_z \,\mathrm{d}s$$

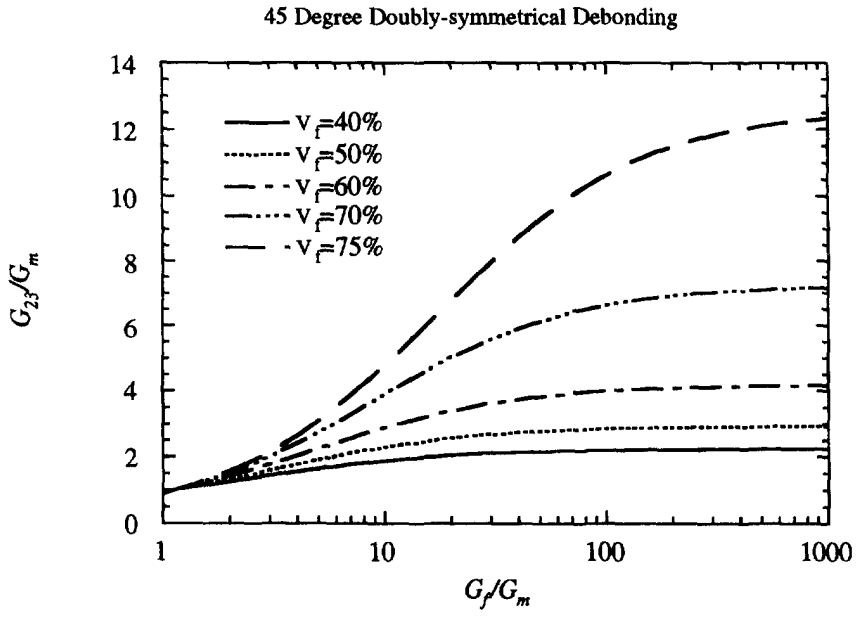

Fig. 15. Effect of fiber volume fraction on the composite shear moduli G_{23} for doubly-symmetrically 45° debonded interface.

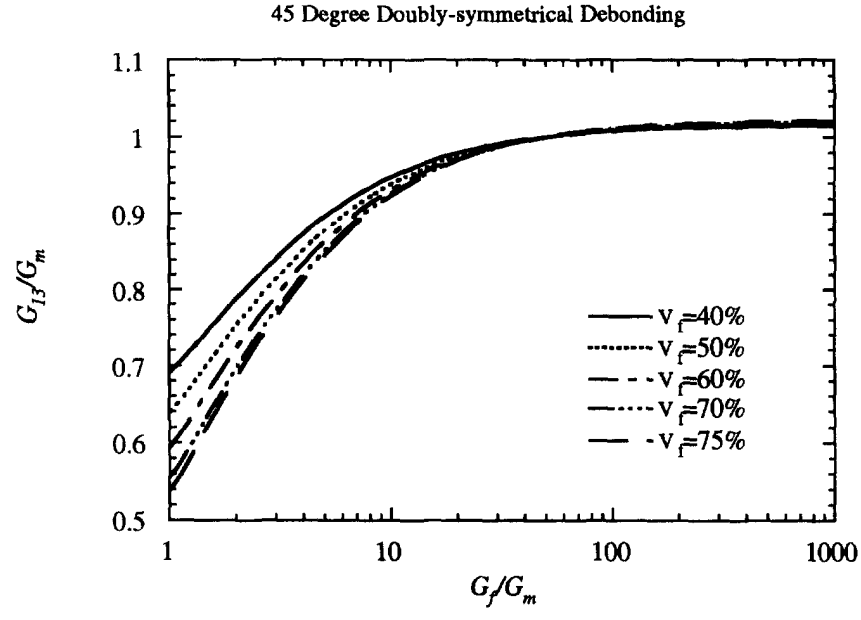

Fig. 16. Effect of fiber volume fraction on the composite shear moduli G_{13} for doubly-symmetrically 45° debonded interface.

$$\bar{\tau}_{xz} = \frac{1}{4ab}\oint xT_z \, \mathrm{d}s.$$

For doubly-symmetric debonding, the integral can be evaluated along the whole outer boundaries of the quarter cell; while for uni-symmetric debonding, the integral is required to be evaluated along the entire outer boundaries of the half cell.

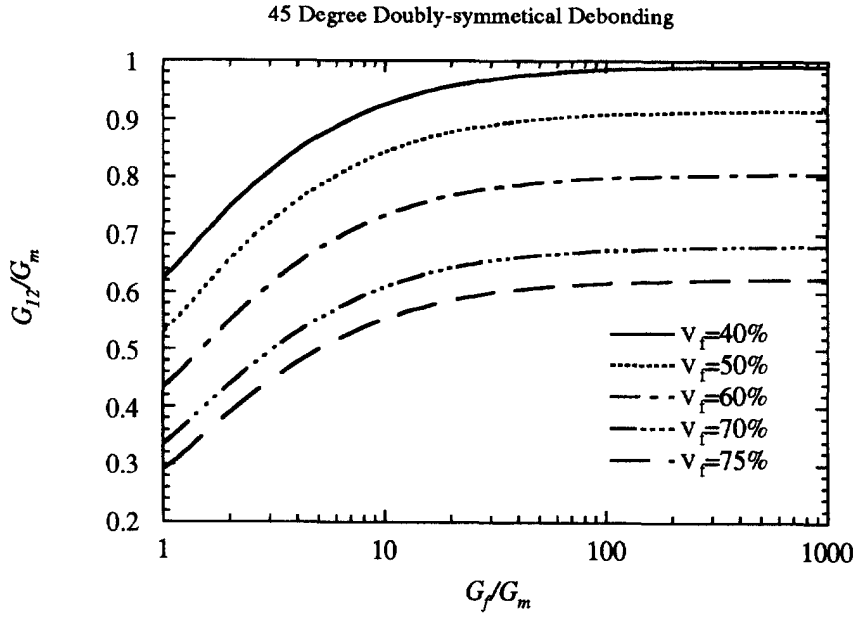

Fig. 17. Effect of fiber volume fraction on the composite shear moduli G_{12} for doubly-symmetrically 45° debonded interface.

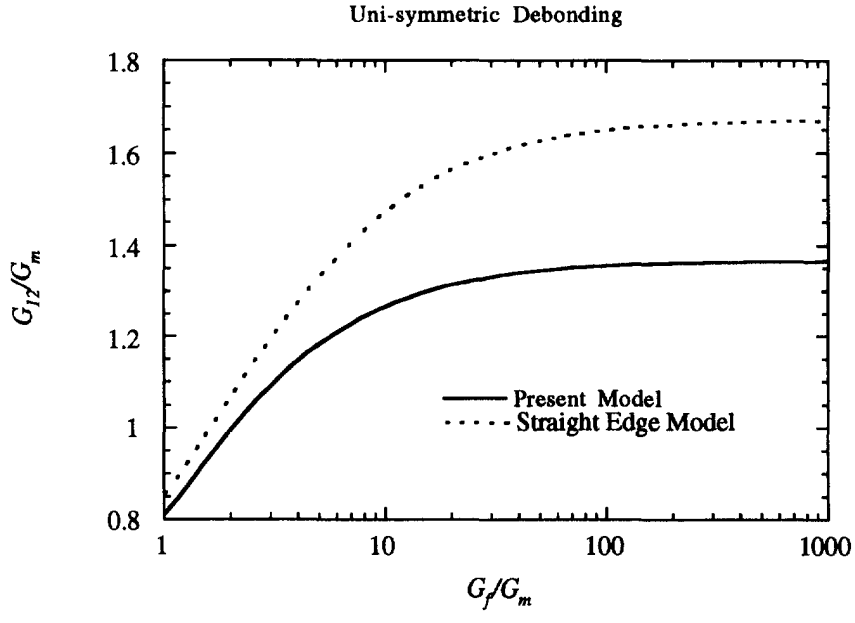

Fig. 18. The comparison of shear moduli G_{12} for 45° uni-symmetric debonding present model vs straight edge model.

The comparison of the shear moduli between the two models is illustrated in Figs 18–23 for different ratios G_f/G_m with a fixed fiber volume fraction $V_f = 40\%$. Figures 18–20 are for uni-symmetric debonding case; Figs 21–23 for doubly-symmetric debonding case. As expected, the straight boundary deformation model gives composite shear moduli upper bound values, in particular the model overestimates the in-plane shear moduli over 20%. In these studies which are not shown in the figures, the disparity between the two models increases dramatically as the fiber volume fraction and/or debonding angle increases.

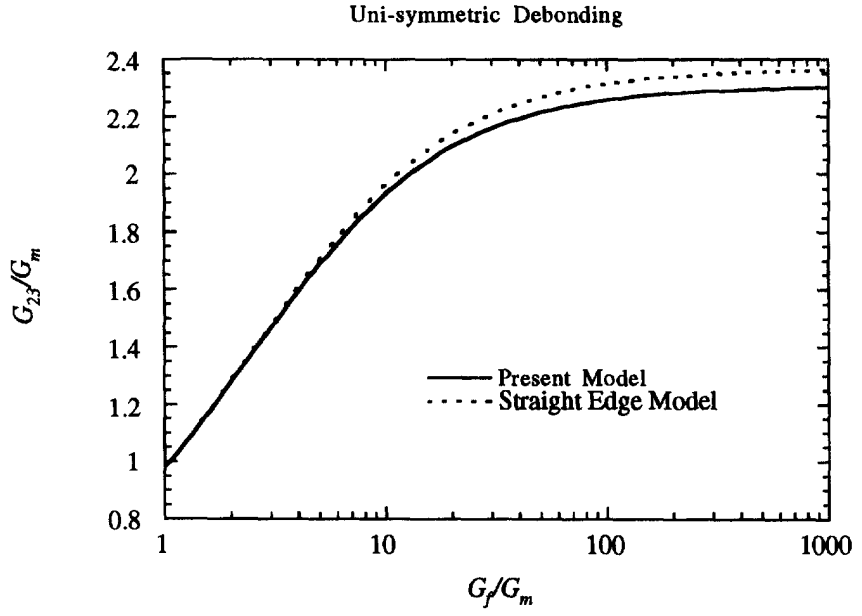

Fig. 19. The comparison of shear moduli G_{23} for 45° uni-symmetric debonding present model vs straight edge model.

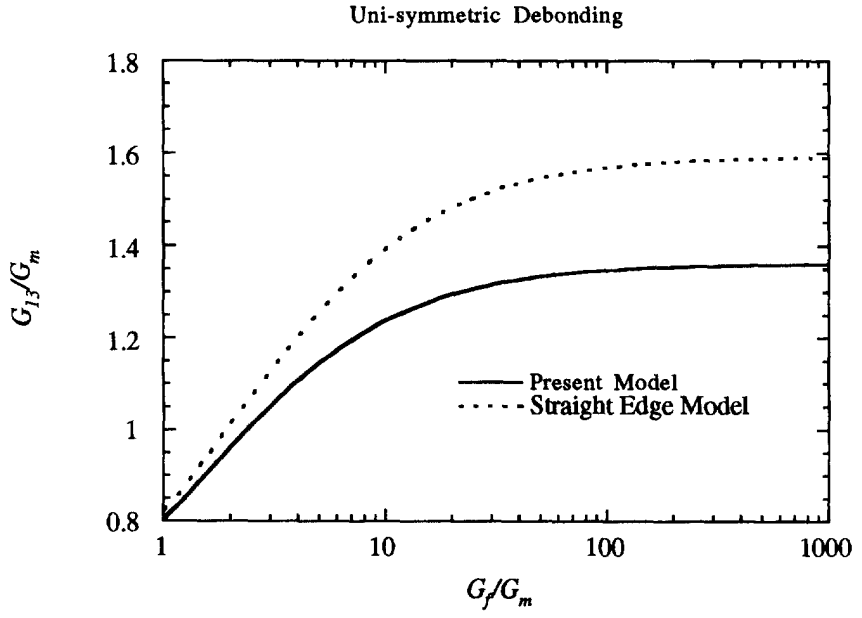

Fig. 20. The comparison of shear moduli G_{13} for 45° uni-symmetric debonding present model vs straight edge model.

CONCLUSIONS

The effect of interfacial debonding on the composite moduli is studied using two-dimensional finite element methods. A periodic rectangular array is assumed in the micro-mechanics analysis. The traction and displacement compatibility conditions along the boundaries of RVE are imposed as the boundary conditions in the finite element analysis. For the case of uni-symmetric or doubly-symmetric interfacial debonding and debonding

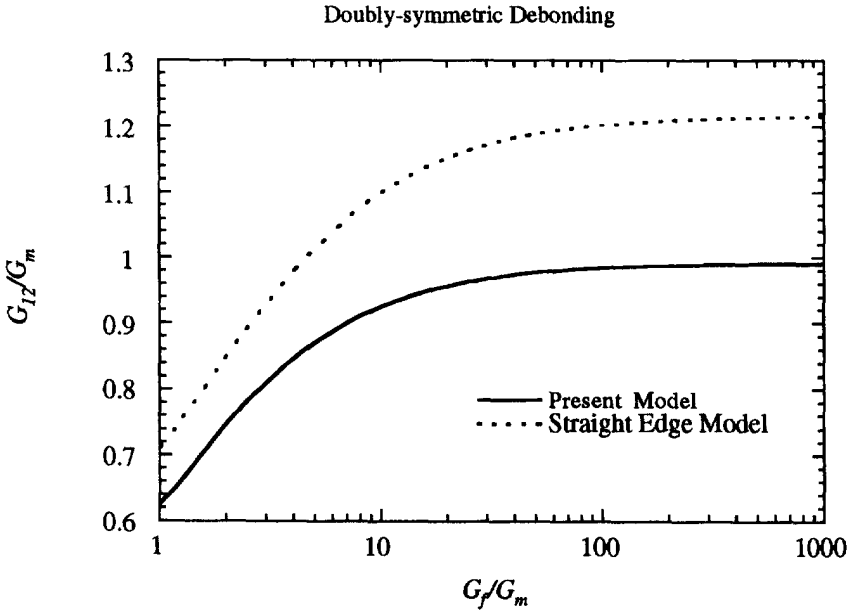

Fig. 21. The comparison of shear moduli G_{12} for 45° doubly-symmetric debonding present model vs straight edge model.

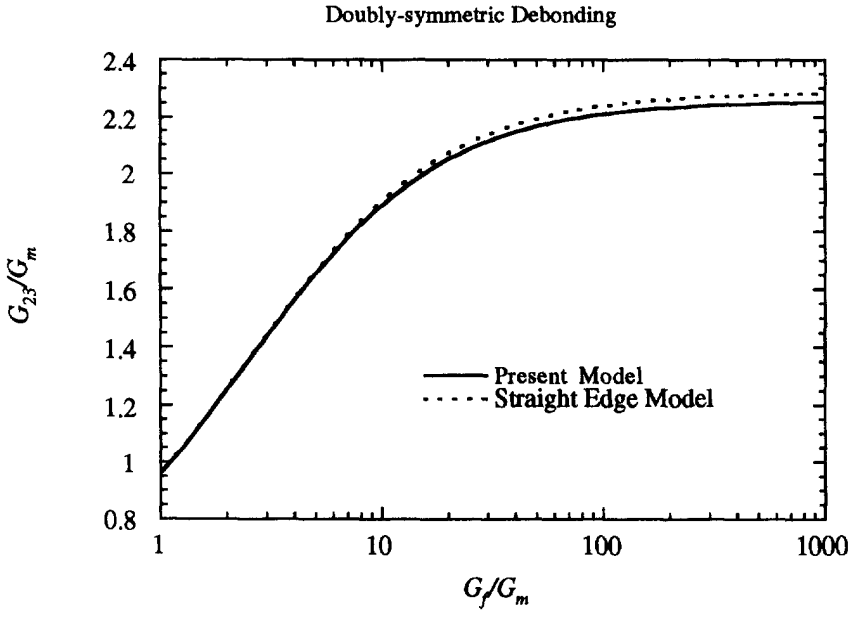

Fig. 22. The comparison of shear moduli G_{23} for 45° doubly-symmetric debonding present model vs straight edge model.

being completely separated studied here, the composite behaves macroscopically orthotropic. Therefore nine independent material constants are required to be investigated in assessing the degradation of the composite moduli due to debonding. Further, only a half cell or a quarter cell need to be modeled for uni-symmetric and doubly-symmetric debonding. Since the edge of the RVE does not remain straight under shear, a new definition of composite shear strains based on surface averaging is thus proposed. Based on the numerical analyses, the following conclusions may be drawn: (1) the degree of debonding has very little effect on the axial composite modulus E_3; (2) the transverse Young's modulus E_1 and

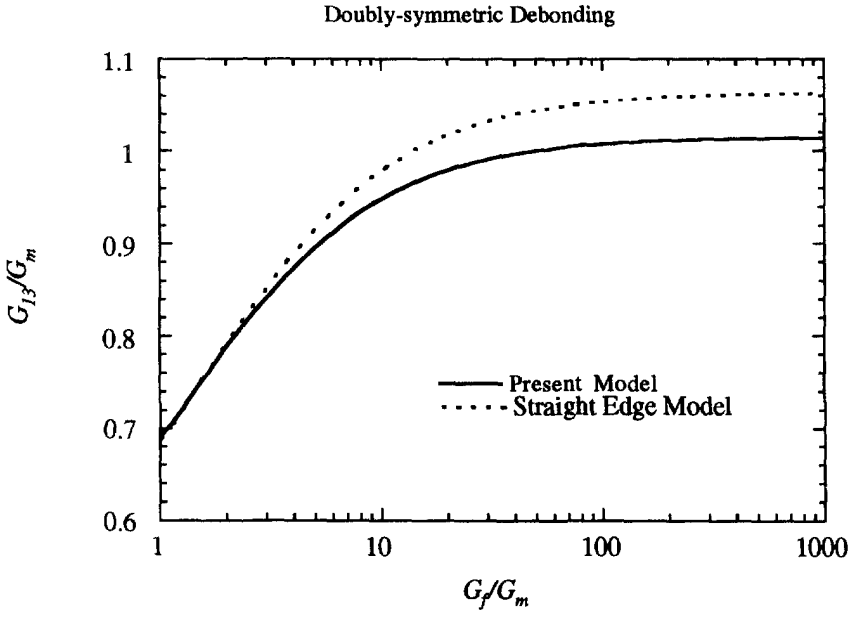

Fig. 23. The comparison of shear moduli G_{13} for 45° doubly-symmetric debonding present model vs straight edge model.

longitudinal shear modulus G_{13}, in-plane shear modulus, G_{12}, and the Poisson's ratio, v_{12}, are affected significantly by the degree of the debonding. This phenomenon is mainly due to the lack of stress transfer across the debonded surfaces from the loading; (3) for all the cases studied, the composite shear moduli approach an asymptote as the ratios of G_f/G_m are very large.

Acknowledgements The first author gratefully acknowledges the financial support under the Air Force Office of Scientific Research (AFOSR) Summer Research Program and under Grant No. MSS-9202223 from the National Science Foundation.

REFERENCES

Adams, D. F. and Doner, D. R. (1967). Longitudinal shear loading of a unidirectional composite. *J. Composite Mat.* **1**, 4–17.

Adams, D. F. and Doner, D. R. (1967). Transverse normal loading of a unidirectional composite. *J. Composite Mat.* **1**, 152–164.

Benveniste, Y. (1984). On the effect of debonding on the overall behavior of composite materials. *Mech. Mat.* **3**, 349–358.

Benveniste, Y. (1985). The effective mechanical behavior of composite materials with imperfect contact between the constituents. *Mech. Mat.* **4**, 197–208.

Chao, R. and Laws, N. (1992). Closure on an arc crack in an isotropic homogeneous material due to uniaxial loading. *Quart. J. Mech. Appl. Math.* **5**, 629–640.

Chen, C. H. and Cheng, S. (1967). Mechanical properties of fiber reinforced composites. *J. Composite Mat.* **1**, 30–40.

Chen, C. H. (1970). Fiber-reinforced composites under longitudinal shear loading. *ASME J. Appl. Mech.* **37**, 198–201.

Chen, C. H. (1971). Rectangular or square array fibrous composite with anisotropic or isotropic filament. *ASME J. Appl. Mech.* **38**, 710–712.

Christensen, R. M. and Lo, K. M. (1979). Solutions for effective shear properties of three-phase sphere and cylinders. *J. Mech. Phys. of Solids* **37**, 315–330.

Foye, R. L. (1966). An evaluation of various engineering estimates of the transverse properties of unidirectional composites. *Proc. 10th National Symp.—Advanced Fibrous Reinforced Composites*, San Diego, pp. G31–42.

Grande, D. H., Mandell, J. F. and Hong, K. C. C. (1988). Fiber-matrix bond strength studies of glass, ceramic, and metal matrix composites. *J. Materials Science* **23**, 11–328.

Hashin, Z. and Rosen, B. W. (1964). The elastic moduli of fiber reinforced materials. *ASME J. Applied Mech.* **31**, 223–232.

Hashin, Z. (1990). Thermoelastic properties of fiber composites with imperfect interface. *Mech. Mat.* **8**, 333–348.

Heaton, M. D. (1968). A calculation of the elastic constants of a unidirectional fibre-reinforced composite. *British J. Appl. Physics Ser.* 2 **1**, 1039–1048.

Hill, R. (1965). A self consistent mechanics of composite materials. *J. Mech. Phys. Solids* **13**, 213–222.

Pagano, N. J. and Tandon, G. P. (1990). Modeling of imperfect bonding in fiber reinforced brittle matrix composites. *Mech. Mat.* **9,** 49–64.

Prewo, K. M. and Brennan, J. J. (1980). High-strength silicon carbide fiber-reinforced glass matrix composites. *J. Mat. Science* **15,** 463–468.

Rice, R. W. (1981). Mechanisms of toughening in ceramic matrix composites. *Ceramic Engng and Science Proc.* **2,** 661–701.

Shimansky, R. A., Hahn, H. T. and Salamon, N. J. (1989). The effect of weak interface on transverse properties of a ceramic matrix composite. In *Interfaces in Composites, Materials Research Society Symposium Proceedings* (eds C. C. Pantano and Eric J. H. Chen), Vol 170, pp. 193–204.

Sokolnikoff, I. S. (1956). *Mathematical Theory of Elasticity*, Second Edition, McGraw-Hill Book Company, New York.

Sun, C. T. and Vaidya, R. S. (1993). On predicting elastic moduli and plastic flow in composite materials using micromechanics. In *The ASC 8th Technical Conference on Composite Materials*, Cleveland, pp. 841–849.

Takahashi, K. and Chou, T.-W. (1988). Transverse elastic moduli of unidirectional fiber composites with interfacial debonding. *Metallurgical Trans. A* **19,** 129–135.

Tso, F. K. and Loomis, W. C. (1982). Micromechanical modeling of 3D composites with interface failure. In *Thermomechanical Behavior of High-Temperature Composites* (ed. J. Jortner) ASME, AD-04, pp. 91–109.